Systematic ^{63}Cu NQR study of the stripe phase in $La_{1.6-x}Nd_{0.4}Sr_xCuO_4$ for $0.07 \leqslant x \leqslant 0.25$

P. M. Singer, A. W. Hunt, A. F. Cederström, and T. Imai
Department of Physics and Center for Materials Science and Engineering, Massachusetts Institute of Technology, Cambridge, Massachusetts 02139
(Received 10 June 1999)

We demonstrate that the integrated intensity of ^{63}Cu nuclear quadrupole resonance (NQR) in $La_{1.6-x}Nd_{0.4}Sr_xCuO_4$ decreases dramatically below the charge-stripe ordering temperature T_{charge}. Comparison with neutron and x-ray scattering indicates that the wipeout fraction $F(T)$ (i.e., the missing fraction of the integrated intensity of the NQR signal) represents the charge-stripe order parameter. The systematic study reveals bulk charge-stripe order throughout the superconducting region $0.07 \leqslant x \leqslant 0.25$. As a function of the reduced temperature $t \equiv T/T_{charge}$, the temperature dependence of $F(t)$ is sharpest for the hole concentration $x \sim 1/8$, indicating that $x \sim 1/8$ is the optimum concentration for stripe formation. [S0163-1829(99)03546-8]

I. INTRODUCTION

Research into the stripe phase of the CuO_2 plane has continued to expand[1–6] since its experimental discovery in 1995 by Tranquada *et al.*[7] Static charge-stripe order was observed for $La_{1.6-x}Nd_{0.4}Sr_xCuO_4$ with $x=0.12$ (Ref. 8) with an onset temperature $T_{charge} \sim 65$ K using neutron diffraction. The same charge-order superlattice peaks were recently confirmed using hard x-ray diffraction by Zimmerman *et al.*[9] and a similar $T_{charge} \sim 70$ K was found. Even more recently, charge-order superlattice peaks have been observed in $La_{1.45}Nd_{0.4}Sr_{0.15}CuO_4$ by Niemöller *et al.*[10] using hard x-rays, and they report a slightly lower onset temperature $T_{charge} \sim 62$ K. Charge transport studies of $La_{1.6-x}Nd_{0.4}Sr_xCuO_4$ by Noda *et al.*[11] also support a static charge-stripe picture. The Hall coefficient shows a dramatic decrease starting around T_{charge}, reflecting the one-dimensional nature of the charge transport in the striped phase. Furthermore, the decrease is sharpest around the $x=1/8$ doping where stripe order is believed to be most robust.[7]

The observation of spin-stripe order has been reported for an even wider range of doping. Neutron scattering by Tranquada *et al.*[12] successfully detected static spin-stripe order for $x=0.12$, 0.15, and 0.20 at $T_{spin} \sim$ 50, 45, and 20 K, respectively. These findings have been comfirmed and extended with more recent measurements by Ichikawa *et al.*[13] The neutron scattering experiments[12] also observe a decreasing sublattice magnetization away from 1/8 doping, and incommensurabilities that are similar to those for the $La_{2-x}Sr_xCuO_4$ series.[14] The most interesting feature, however, is that the onset temperature T_{spin} for spin-stripe order in $La_{1.6-x}Nd_{0.4}Sr_xCuO_4$ at $x=0.12$ is 50 K, which is *lower* than T_{charge} of 65 K, implying that charge order is a precursor to spin order. In addition, a spin ordering temperature $T_{spin}=30$, 25, and $\leqslant 4$ K for $x=0.12$, 0.15, and 0.20, respectively, has been determined by Nachumi *et al.*[15] using muon spin resonance (μSR). The μSR probe has a lower inherent frequency ($\sim 10^7$ Hz) compared with elastic neutron scattering ($\sim 10^{11}$ Hz), so the discrepency in the spin ordering temperature between the μSR and neutron results indicates that the spin-stripe fluctuations gradually slow down with decreasing temperature below T_{charge}. That is, spin-stripe ordering is a glassy transition in $La_{1.6-x}Nd_{0.4}Sr_xCuO_4$.

In this paper, we utilize Cu nuclear quadrupole resonance (NQR) to probe stripe instabilities in $La_{1.6-x}Nd_{0.4}Sr_xCuO_4$. Cu NQR gives unique information about the charge environment at the Cu nuclear site. In particular, the resonance frequency for Cu NQR, conventionally called ν_Q (~ 36 MHz),[16,17] is determined by the energy splitting of the $\pm\frac{3}{2} \leftrightarrow \pm\frac{1}{2}$ levels, which in turn is directly proportional to the electric field gradient (EFG) at the Cu nuclear site. The EFG itself is very sensitive to the charge environment, and we thus expect any change in the charge distribution within the CuO_2 plane, such as charge density waves (CDW), to directly affect Cu NQR. Earlier work on conventional CDW systems such as $NbSe_3$ (Ref. 18) and $Rb_{0.3}MoO_3$ (Ref. 19) made use of the extreme sensitivity of ν_Q to the EFG. Our approach[1] makes use of wipeout effects[20] in ^{63}Cu NQR from which we obtain unique information about charge-stripe order in $La_{1.6-x}Nd_{0.4}Sr_xCuO_4$. The fundamental difference between NQR and neutron scattering is that the former is a local probe, while the latter requires spatial coherence; thus NQR and neutron scattering provide complimentary information about stripe physics. The NQR wipeout alone cannot give details of the spatial structure of the stripes, but as a local probe, NQR is very sensitive to charge stripes with short or poorly defined correlation lengths. Indeed, away from the robust 1/8 region, detection of charge stripes by bulk scattering has proved difficult and up to now, no direct observation of charge-stripe order has been reported other than for $La_{1.48}Nd_{0.4}Sr_{0.12}CuO_4$ and $La_{1.45}Nd_{0.4}Sr_{0.15}CuO_4$. However, by confirming that the NQR wipeout fraction $F(T)$ has *identical* temperature dependence as the neutron and x-ray charge-stripe order parameter for $x=0.12$ and 0.15, we claim that $F(T)$ is the charge-stripe order parameter and we extend the detection of charge-stripe order in $La_{1.6-x}Nd_{0.4}Sr_xCuO_4$ to $0.07 \leqslant x \leqslant 0.25$. We also establish that the transition is sharpest at $x=0.12$.

The rest of the paper is presented as follows: in Sec. II we go over the experimental details and present our results. In Sec. III we discuss our NQR data in comparison with the

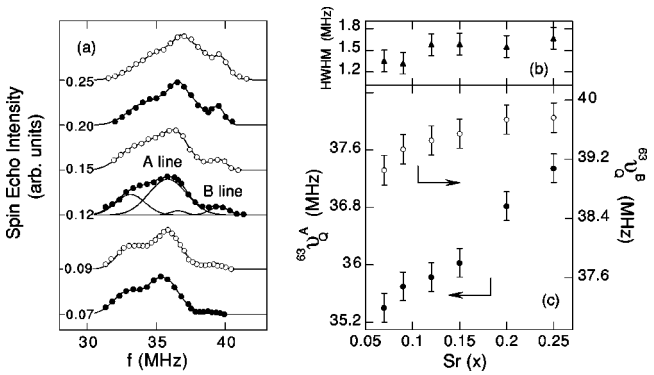

FIG. 1. (a) Line shapes for $La_{1.6-x}Nd_{0.4}Sr_xCuO_4$ where the value $0.07 \leqslant x \leqslant 0.25$ is shown for each line. All line shapes were taken at 150 K and all are normalized to equal heights for purposes of comparison. The raw data points are shown along with their fits (see text) and the decomposition of the fit for $x=0.12$ is shown. (b) ^{63}Cu A line HWHM (▲) obtained by fitting the 150 K line shapes. (c) A line $^{63}\nu_Q$ (●), B line $^{63}\nu_Q$ (○), both at 150 K.

neutron and x-ray measurements. Section IV contains the conclusions.

II. EXPERIMENTAL PROCEDURES AND RESULTS

A. Sample preparation

Powder samples of $La_{1.6-x}Nd_{0.4}Sr_xCuO_4$ with $x=0.07$, 0.09, 0.12, 0.15, 0.20, and 0.25 were prepared by solid-state reactions of La_2O_3 (99.99%), Nd_2O_3 (99.99%), $SrCO_3$ (99.99%) and CuO (99.995%). The materials were mixed in the desired stochiometry and prereacted at 850 °C. The samples were then finely ground and heated to 950 °C. This cycle was repeated several times. For the final reaction, the powder was pressed (0.6 GPa) into rods of cylindrical shape and annealed in flowing oxygen. The heat cycle for this final reaction was similar to that used by Breuer *et al.*[21] where a highest temperature of 1150 °C was used. All the samples were confirmed by x-ray diffraction to be single phased, and the room temperature orthorhombic splitting $[b-a]$ was in good agreement with (Ref. 21).

B. Characterization of NQR spectra

The ^{63,65}Cu NQR frequency spectra, or line shapes, were measured using a 90°-τ-180°-τ-echo phase-cycled pulse sequence at fixed τ. The resonant circuit was heavily damped so that short τ could be used (typically $\tau=10$–12 μs). In addition, the damping assured that the Q value of the resonance circuit changed little with temperature; therefore pulse conditions and sensitivity remained constant.

Figure 1(a) shows the line shapes for all the $La_{1.6-x}Nd_{0.4}Sr_xCuO_4$ materials observed at 150 K. At 150 K, all the materials are in the LTO (low-temperature orthorhombic) phase. The two different sites, conventionally called A and B, are present for all the materials and each is further split into two lines due to the presence of ^{63}Cu and ^{65}Cu isotopes. Note that the intensity of the B line compared with that of the A line goes roughly as the doping x, in good agreement with earlier reports by Yoshimura *et al.*[22] It is generally believed that the B line originates from Cu nuclei underneath a Sr atom, and the A line from the Cu nuclei away from the Sr dopants. This picture is consistent with the observed ratio of intensities. We also observed an enhanced tail at the lower frequency side of the spectrum, possibly from Cu sites underneath a Nd atom. This lower frequency tail is also observed in $La_{1.8-x}Eu_{0.2}Sr_xCuO_4$ spectra,[23] presumably from Cu sites underneath a Eu atom.

In order to extract quantitative information about the line shapes, each spectrum was fit to a convolution of Gaussians: two for the ^{63}Cu and ^{65}Cu A line, and two for the ^{63}Cu and ^{65}Cu B line [as shown for $x=0.12$ in Fig. 1(a)]. Fitting the A line with two Gaussians results in six parameters (two amplitudes, two peak positions corresponding to the NQR frequencies $^{63}\nu_Q$ and $^{65}\nu_Q$, and two widths). Using the known ratios of $^{63}\nu_Q/^{65}\nu_Q = Q^{63}/Q^{65} = 1.083$ and $N^{63}/N^{65} = 69/31$ for the quadrupole moments Q and isotopic abundances N, respectively, reduces the number of free parameters. The B line was fit in the same manner.

Results of A line half width at half maximum (HWHM) observed at 150 K are shown in Fig. 1(b). The fitted value of the HWHM is sensitive to the line-shape data, especially at the tails, but the general trend is that the HWHM increases with x. The value is generally 50% higher than the HWHM observed for $La_{2-x}Sr_xCuO_4$ at the same doping.[1] This is possibly due to the increase in structural disorder due to Nd substitution.

Results of the $^{63}\nu_Q$ for the A and B lines observed at 150 K are shown in Fig. 1(c). The doping dependence of ν_Q for the A and B lines in $La_{1.6-x}Nd_{0.4}Sr_xCuO_4$ is consistent with previous studies on $La_{2-x}Sr_xCuO_4$.[21]

C. Temperature dependence of ^{63}Cu NQR spectra

The temperature dependence of the line shapes came in three forms:

(1) The inhomogeneous linewidth (HWHM) of the ^{63}Cu A line shown in Fig. 2(a) for $x=0.12$ shows a smooth increase ($\sim$20%) from 300 to 20 K. The same temperature dependence of the HWHM was found for all the samples. The HWHM data were used to estimate the integrated intensity of the NQR line shape, so to avoid unnecessary scatter in this estimation, we typically used a linear fit to the HWHM.

(2) Figure 2(a) shows the temperature dependence of $^{63}\nu_Q$ for the $x=0.12$ sample, and as can be seen, $^{63}\nu_Q$ shows a gradual increase of several hundred kHz from room temperature down to $T_{charge}=70(7)$ K, below which the rise in $^{63}\nu_Q$ is more dramatic. The other samples show qualitatively similar temperature dependence, as discussed in Sec. III.

(3) All of the materials showed a dramatic loss of signal intensity at temperatures below 150 K. Figure 2(b) shows the temperature dependence of the line shapes for $x=0.12$. The NQR intensity is proportional to the statistical Boltzmann factor $e^{h\nu_Q/k_BT} \sim 1/T$, where $h\nu_Q \ll k_BT$ in the present case. Accordingly, we multiplied each line shape by T to take this into account. The loss of NQR intensity therefore implies that ^{63,65}Cu nuclear spins in certain segments of the sample become undetectable.

In order to quantify the loss of signal shown in Fig. 2(b), we estimated the temperature dependence of the integrated intensity for each material using a three step process. (1) We calculated the area of the line shape from the fitting procedure described above. (2) A Boltzmann factor was included

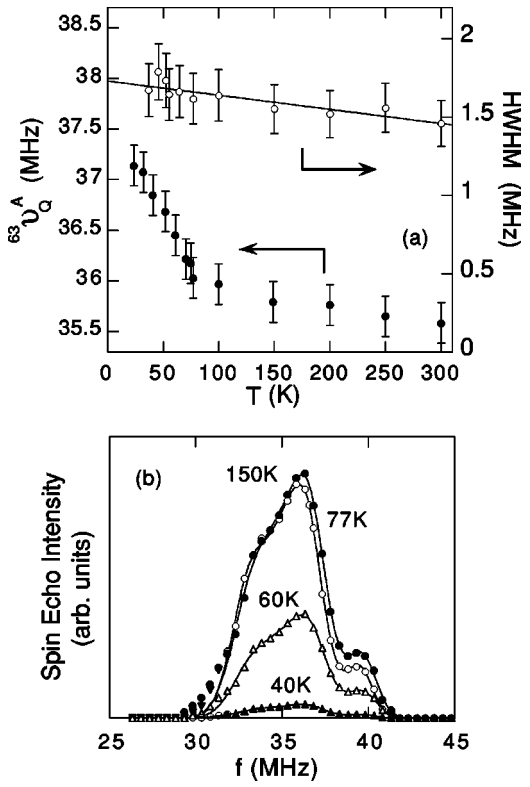

FIG. 2. (a) Temperature dependence of the ^{63}Cu A line HWHM for $x=0.12$ (○) along with a linear extrapolation, and the temperature dependence of A line $^{63}\nu_Q$ for $x=0.12$ (●). (b) $x=0.12$ line shapes at 150 K (○), 77 K (●), 60 K (△), and 40 K (▲), all corrected for Boltzmann factor (see text).

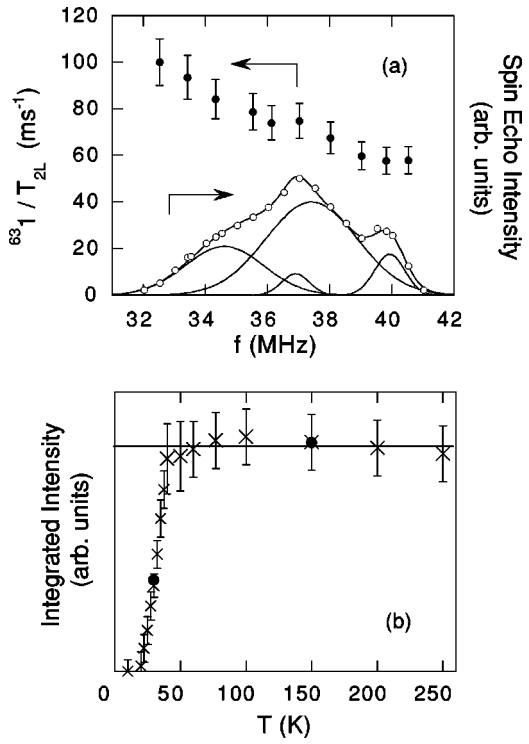

FIG. 4. (a) $^{63}1/T_2$ in ms^{-1} (●) as a function of frequency at 30 K for the $x=0.20$ sample. Also shown, the 30 K line shape in arbitrary units measured at fixed $\tau=0.12$ μs (○) along with its fit and the decomposition of the fit. (b) Temperature dependence of the integrated intensity for $x=0.20$ measured by the full T_2 correction (●), or by correcting for T_2 just at the peak of the A line (×).

at each temperature. (3) The line shapes were corrected for spin echo decay as described below. We also attempted to make standard NQR frequency corrections of $1/f^2$ to the line shape intensity,[17] but they did not affect our results. Figure 3(a) shows the results of the temperature dependence of the integrated intensity for $x=0.12$. When working out the line-shape area, only the integral of the A line intensity was used so that unnecessary scattering of the estimated total intensity was avoided. This was justified by previous high precision studies of the NQR intensity[1] on a related compound $La_{1.875}Ba_{0.125}CuO_4$ enriched with the ^{63}Cu isotope. As shown in Fig. 3(b), both A and B lines have identical temperature dependence of the integrated NQR intensity.

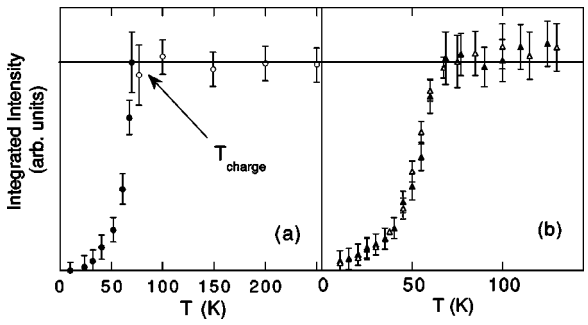

FIG. 3. (a) Temperature dependence of the integrated ^{63}Cu NQR intensity for $La_{1.48}Nd_{0.4}Sr_{0.12}CuO_4$ in arbitrary units. Also shown, the onset temperature for wipeout T_{charge}, and the (○) show Gaussian curvature in the spin echo decay; (●) do not (see text). (b) Temperature dependence of the integrated intensity for $La_{1.875}Ba_{0.125}CuO_4$ for the A line (△) and B line (▲).

Corrections for spin-echo decay, or the ''T_2 corrections,'' were made by measuring the spin-spin relaxation $1/T_2$ (Ref. 17) at each temperature. Since T_2 exhibits slight dependence on frequency, in order to be rigorous one needs to make corrections for T_2 at every frequency rather than just at the peak of the A line. We tested whether the rigorous approach was necessary. For the $x=0.20$ sample, the effect of T_2 was nearly uniform across the entire line shape at 150 K, but at 30 K [shown in Fig. 4(a)], $1/T_2$ increased towards the lower frequency side. Figure 4(b) shows the integrated intensity with the ''full T_2 correction'' at 150 and 30 K compared with the intensity points deduced from correcting for T_2 just at the peak frequency. Both methods gave the same results within experimental error, so we conclude that the T_2 correction at the peak of the A line is sufficient.

As shown in Fig. 3(a) for $x=0.12$, the intensity is constant within experimental error from 300 to 70(7) K, but then shows a dramatic drop to zero from 70(7) to 10 K. This is the 'wipeout' effect, and we will discuss the mechanism of the wipeout in Sec. III. By taking the constant value between 300 and 70(7) K as the zero baseline and then inverting the plot, one obtains the fraction of signal lost, or the wipeout fraction $F(T)$. As we demonstrate in Sec. III, the onset temperature of $F(T)$ is in good agreement with the charge-stripe ordering temperature T_{charge} determined by neutron/x-ray scattering. Figure 5 is a plot of the temperature dependence of $F(T)$ for all the $La_{1.6-x}Nd_{0.4}Sr_xCuO_4$ samples. Even though T_{charge} and the transition widths are different for

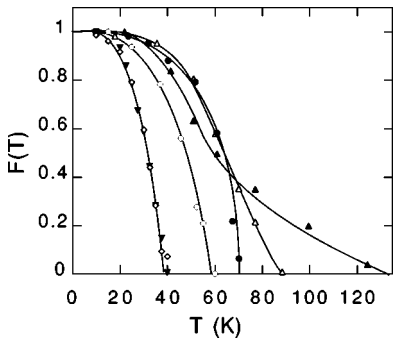

FIG. 5. Wipeout fraction $F(T)$ in $La_{1.6-x}Nd_{0.4}Sr_xCuO_4$ for $x=0.07$ (▲), $x=0.09$ (△), $x=0.12$ (●), $x=0.15$ (○), $x=0.20$ (▼), and $x=0.25$ (◇). The solid lines through the points are a guide for the eye.

various x, all show 100% wipeout, thus leaving no observable ^{63}Cu NQR signal by ~ 10 K. We emphasize that since we have taken T_2 corrections into account for the integrated intensity, the loss of observable NQR signal is *not* caused by a divergence of T_2 throughout the entire sample, as is often observed in the vicinity of magnetic long range order.

D. ^{63}Cu spin-lattice relaxtion

Figure 6 shows the spin-lattice relaxation rate $^{63}1/T_1$ for $La_{1.48}Nd_{0.4}Sr_{0.12}CuO_4$, $La_{1.45}Nd_{0.4}Sr_{0.15}CuO_4$, and $La_{1.68}Eu_{0.2}Sr_{0.12}CuO_4$, in addition to $La_{1.885}Sr_{0.115}CuO_4$ data from (Ref. 23). All $^{63}1/T_1$ were taken at A line $^{63}\nu_Q$, and all fit well to single exponential recoveries as expected for $I=3/2$ nuclei in NQR. The relaxation rates for the four materials are equal within 10% from 300 K to about 125 K, but below about 125 K, the $^{63}1/T_1$ data for $La_{1.6-x}Nd_{0.4}Sr_xCuO_4$ measured for the remaining ^{63}Cu NQR signal increases with deceasing temperature as $\sim 1/T$. The $^{63}1/T_1$ data for $La_{1.68}Eu_{0.2}Sr_{0.12}CuO_4$ (Ref. 23) start to increase at a lower temperature of 35(5) K. Wipeout effects below 30 K prohibit further measurement of $^{63}1/T_1$ data for $La_{1.6-x}Nd_{0.4}Sr_xCuO_4$ and $La_{1.68}Eu_{0.2}Sr_{0.12}CuO_4$. At 30 K, even though $^{63}1/T_1$ from the remaining $\sim 5\%$ of the signal is increasing with decreasing temperature, it is still measurable.

E. ^{63}Cu spin-echo decay

The NQR spin-echo intensity $S(2\tau)$ depends strongly on 2τ (where τ is the time separation between the 90° and 180° pulses) as shown in Fig. 7 where $S(2\tau)$ is plotted on a logarithmic scale. The data are from the $La_{1.48}Nd_{0.4}Sr_{0.12}CuO_4$ sample, and $S(2\tau)$ is measured at $^{63}\nu_Q$ for the A line at each temperature. In order to correct the NQR integrated intensity for spin-echo decay, one has to extrapolate the curve to the zero time $2\tau=0$. Most importantly, qualitative changes of the decay shape (such as loss of Gaussian curvature below T_{charge}) makes T_2 corrections essential in determining T_{charge} accurately. The shortest possible 2τ is limited by the the circuit dead time with a value of ~ 20 μs.

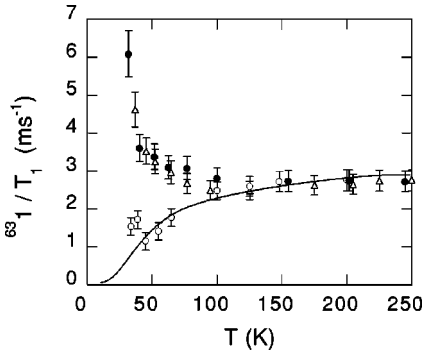

FIG. 6. $^{63}1/T_1$ temperature dependence for $La_{1.48}Nd_{0.4}Sr_{0.12}CuO_4$ (●), $La_{1.45}Nd_{0.4}Sr_{0.15}CuO_4$ (△), $La_{1.68}Eu_{0.2}Sr_{0.12}CuO_4$ (○), and the solid line $La_{1.885}Sr_{0.115}CuO_4$ (Ref. 23), all measured in ms^{-1}.

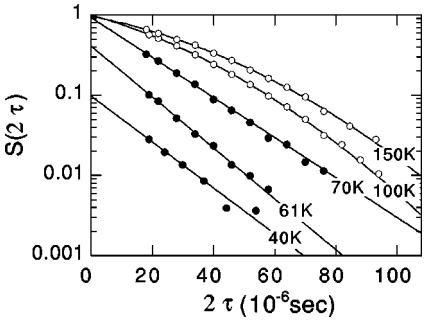

FIG. 7. Spin-echo decay for $La_{1.48}Nd_{0.4}Sr_{0.12}CuO_4$ at the various temperatures normalized by the Boltzmann factor. Also shown are spin-echo envelopes fit with Gaussian curvature (○), and without (●).

The fit used for the extrapolation has the functional form

$$S(2\tau)=S(0)e^{-2\tau/T_{2L}}e^{-(2\tau)^2/2T_{2G}^2}, \tag{1}$$

where T_{2L} is the Lorentzian decay which has contributions from the Redfield T_1 process, and T_{2G} is the Gaussian decay which is dominated by the indirect spin-spin coupling between like spins.[17] In various high-T_c and related copper oxides, when the NQR linewidth is as small as ~ 200 kHz, one can excite the entire ^{63}Cu NQR spectrum with intense rf pulses. In such cases, one can give theoretical constraints on the Lorentzian contribution T_{2L} based on calculations of the spin-lattice relaxation process.[24] In the present case, however, the full NQR linewidth (~ 3 MHz) is an order of magnitude larger than the strength of the rf pulses (~ 200 kHz). It is well known that this gives rise to artificial changes in the functional form of the spin-echo decay,[25] making the Gaussian contribution more Lorentzian. Accordingly, we chose both T_{2L} and T_{2G} as free parameters. We note that use of the stretched exponential form of the fitting function

$$S(2\tau)=S(0)e^{-(2\tau/T_2)^\beta}, \tag{2}$$

often used in the literature under similar circumstances did not affect our estimate of the temperature dependence of $S(0)$.

At T_{charge} and below, the spin-echo decay dramatically changed to a single rate Lorentzian. This can be seen by the loss of curvature in Fig. 7. As discussed in Sec. III, this crossover provides an added signature for the onset of wipeout, however the crossover also generates more potential error in the estimate of the T_2 corrected intensity $S(0)$. Small changes of curvature in the fit create large variations in the value of $S(0)$ at $T \gtrsim T_{charge}$, so extra care had to be taken for data measurements and fits around T_{charge}. This com-

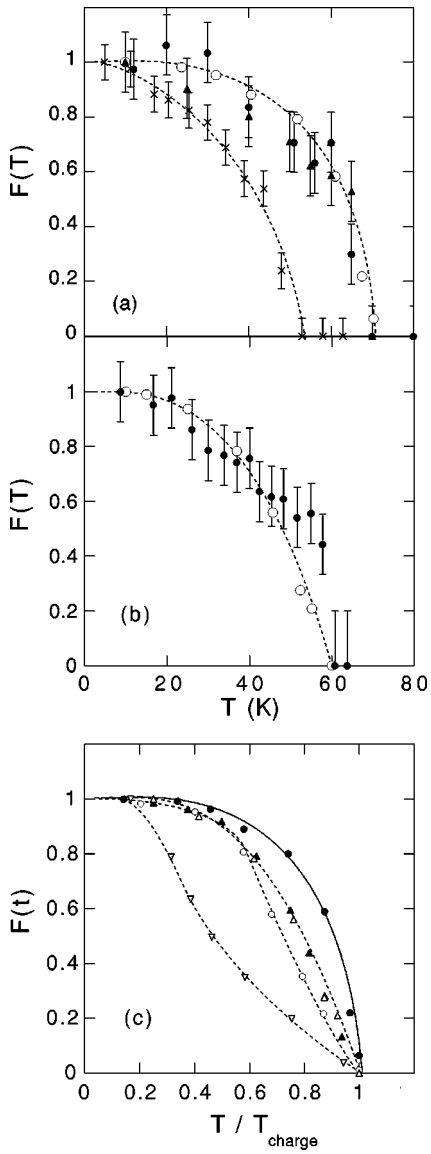

FIG. 8. (a) Plots of the wipeout fraction $F(T)$ (○), the neutron charge order parameter (Ref. 8) (●), the x-ray order parameter (Ref. 9) (▲), and the neutron spin order parameter (Ref. 8) (×) for $x=0.12$. Each data set is normalized to its 10 K value and the dotted lines are guides for the eye. (b) Wipeout fraction $F(T)$ (○) along with the x-ray order parameter (Ref. 10) (●) for $x=0.15$. Each data set is normalized to its 10 K value and the dotted line is a guide for the eye. (c) Wipeout fraction $F(t)$ as a function of the reduced temperature $t=T/T_{charge}$ for $x=0.07$ (▽), $x=0.09$ (○), $x=0.12$ (●), $x=0.15$ (△), and $x=0.20$ (▲). The solid line is $f_d(t)$, and the dashed lines are guides for the eye.

plexity is the reason for the larger error bars around T_{charge} in Fig. 3(a). Consequently, T_{charge} is given a $\pm 10\%$ error.

III. DISCUSSION

A. Wipeout effects

We now compare the NQR wipeout fraction $F(T)$ to elastic neutron diffraction studies carried out for $La_{1.48}Nd_{0.4}Sr_{0.12}CuO_4$ by Tranquada *et al.*,[8] where charge-stripe order was discovered. Figure 8(a) is a comparison of the temperature dependence of the square root of the transverse charge-order peak[8] normalized to 10 K, along with our temperature dependence of $F(T)$. We note that, in general, the elastic scattering intensity represents the square of the order parameter [for example, the intensity of the magnetic Bragg scattering is the square of the sublattice magnetization $M(T)$].[26] The identical temperature dependence of $F(T)$ and the neutron charge-order parameter allows us to conclude that the wipeout fraction $F(T)$ represents the charge-stripe order parameter. Also plotted is the square root of the static spin-ordered peaks $M(T)$ for $x=0.12$ by neutron diffraction,[8,12] and it clearly indicates the wipeout fraction is triggered by charge order and not spin order.

Further evidence of charge-stripe order in $La_{1.48}Nd_{0.4}Sr_{0.12}CuO_4$ (Ref. 9) and $La_{1.45}Nd_{0.4}Sr_{0.15}CuO_4$ (Ref. 10) has been reported using high energy x-ray scattering. Figure 8(a) includes the x-ray results for $x=0.12$, where the square roots of the longitudinal charge peaks are plotted, normalized to 10 K. The x-ray data are in good agreement with both neutron and NQR data. Figure 8(b) is a comparison of x-ray data for $x=0.15$,[10] where we have plotted the square root of the charge peaks in the transverse direction and compared it to our wipeout fraction $F(T)$ for $x=0.15$. Again, the x-ray data agree on the onset temperature $T_{charge}\sim 60(6)$ K obtained from NQR. Both sets of x-ray data further support our identification of the wipeout fraction $F(T)$ as the charge-stripe order parameter. Furthermore, we note that T_{charge} measured by NQR, x ray, and neutron *all* agree for $x=0.12$ despite the different frequency scales of each probe, indicating that charge stripes slow down to NQR time scales very quickly near T_{charge}.

Given the evidence for charge-stripe ordering in $La_{1.48}Nd_{0.4}Sr_{0.12}CuO_4$ (Refs. 8 and 9) and $La_{1.45}Nd_{0.4}Sr_{0.15}CuO_4$,[10] we will now argue that the Cu NQR ''wipeout''[20] effect comes as a natural consequence of the ordering. Because the resonant frequency $^{63}\nu_Q$ is directly proportional to the electric field gradient at the Cu site, we expect NQR to be very sensitive to local charge distributions. Indeed, a spatial modulation of the hole concentration ranging from 0 to 0.5 hole per Cu atom results in as much as an ~ 8 MHz (Ref. 21) instantaneous variation of $^{63}\nu_Q$. In the proposed stripe model[7] at $x\sim 1/8$, rivers of hole-rich CuO chains with effectively 0.5 hole per Cu are separated by bare three-leg CuO ladders with no holes. We therefore expect that below the onset temperature for charge-stripe order T_{charge}, regions which contain stripe fluctuations will have instantaneously varying $^{63}\nu_Q$ distributions, and if these fluctuations are on the NQR time scale (i.e., fluctuate at frequencies of order $^{63}\nu_Q$), the resonance condition in those regions will no longer be well defined. Furthermore, charge order turns on slow spin fluctuations[27] resulting in divergences in the spin-lattice $^{63}1/T_1$ (Ref. 28) and spin-spin $^{63}1/T_2$ relaxation rates within the stripe-ordered domains (note that the measured $^{63}1/T_1$ and $^{63}1/T_{2L}$ in Fig. 6 and Fig. 10 do not necessarily reflect the relaxation rates in the ordered segments of the sample but they are a measure of relaxation rates of the segments that have not yet ordered). Both these effects will result in a loss of ^{63}Cu NQR signal intensity and we therefore expect the fraction of the intensity loss to be a good measure of stripe order.

It is worth mentioning that at low enough temperatures, an NQR like signal reappears for the case of

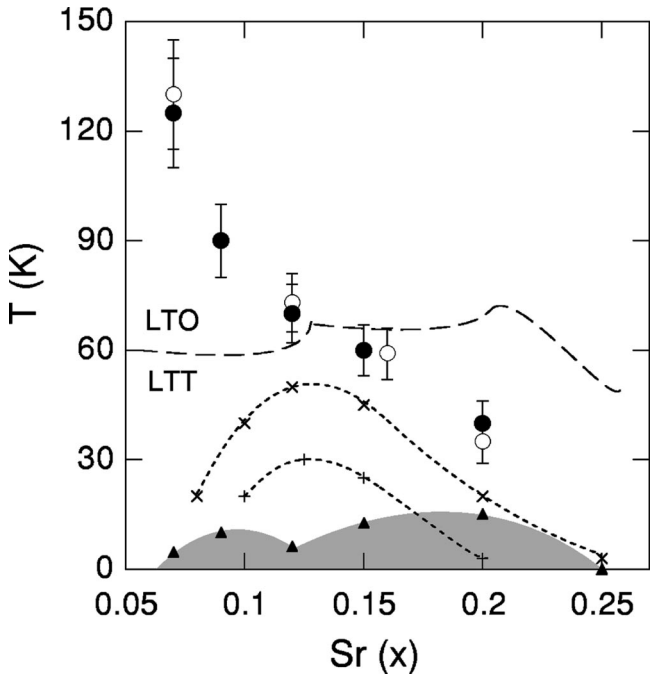

FIG. 9. Phase diagram with T_{charge} for $La_{1.6-x}Nd_{0.4}Sr_xCuO_4$ (●), T_{charge} for $La_{1.8-x}Eu_{0.2}Sr_xCuO_4$ (○), T_{spin} for $La_{1.6-x}Nd_{0.4}Sr_xCuO_4$ according to neutron scattering (×) (Ref. 13), T_{spin} for $La_{1.6-x}Nd_{0.4}Sr_xCuO_4$ according to μSR (+) (Ref. 15), and T_c for $La_{1.6-x}Nd_{0.4}Sr_xCuO_4$ (▲), along with a shaded region to highlight the superconducting phase. Also shown is the LTO to LTT (or LTLO) boundary (broken line) for $La_{1.6-x}Nd_{0.4}Sr_xCuO_4$ (Ref. 33), and two dashed lines joining the (×) and (+) points as a guide for the eye. Near the solubility limit, we find $T_{charge}=40(10)$ K for $La_{1.35}Nd_{0.4}Sr_{0.25}CuO_4$ (not shown) to be about the same as $T_{charge}=40(6)$ K for $La_{1.40}Nd_{0.4}Sr_{0.20}CuO_4$.

$La_{1.88}Ba_{0.12}CuO_4$.[29] Below $\lesssim 10$ K, static magnetic hyperfine fields strongly perturb the Cu NQR spectrum causing a line broadening from low frequencies up to 80 MHz.[29] We confirmed the findings from Ref. 29 for $La_{1.88}Ba_{0.12}CuO_4$, where a broad, featureless Zeeman-perturbed NQR spectrum at 1.7 K was reported. We note that the low-temperature spectrum for $La_{1.6-x}Nd_{0.4}Sr_xCuO_4$ is further complicated by magnetic field contributions from the Nd ions that order at $\lesssim 3$ K.[8]

We now discuss a possible fit of the temperature dependence of $F(T)$. Conventional CDW ground states have many common characteristics with other broken symmetry ground states such as superconducting and spin-density-wave ground states. In particular, within the weak coupling limit, the thermodynamics of the phase transition and the temperature dependence of the order parameter are the same as those of a BCS superconductor.[30,31] To see if this is the case, we present Fig. 8(c) where $F(t)$ is plotted as a function of the reduced temperature $t=T/T_{charge}$ for all the $La_{1.6-x}Nd_{0.4}Sr_xCuO_4$ samples. The solid curve is the BCS form of the condensate density $f_d(t)$ in the dynamic limit,[32] and the dashed curves are a guide for the eye. The data for the $x=0.09$, 0.15, and 0.20 samples look similar, and the $x=0.07$ data stand out as having the broadest transition. The $x=0.25$ data (not shown) look identical to the $x=0.20$ data. The temperature dependence of $F(t)$ for $x=0.12$ appears to be the sharpest and shows the best agreement with $f_d(t)$. From the wipeout mechanism we have proposed, this is expected since $F(T)$ is related to the fraction of the CuO_2 plane where condensate fluctuations exist. The fact that the transition is sharpest around $x\sim 1/8$ could indicate that the charge stripe is most stable around $x\sim 1/8$.

We now present the phase diagram of $La_{1.6-x}Nd_{0.4}Sr_xCuO_4$ in Fig. 9, with T_{charge}, T_{spin} according to neutron scattering,[12] T_{spin} obtained by μSR,[15] the superconducting transition temperature T_c, and the LTO to LTT (low-temperature tetragonal) or LTLO (low-temperature less orthorhombic) transition temperature T_{LTT}.[33] We measured the bulk magnetic susceptibility with a SQUID magnetometer in a field of 10 Oe, and we estimated T_c by taking the slope at the half point in the diamagnetic response and extrapolating to zero susceptibility. The $x=0.12$ and 0.07 samples show residual superconducting components, and the $x=0.25$ sample shows no diamagnetic response down to 3 K. The $x=0.09$, 0.15, and 0.20 samples have the largest low-temperature susceptibility $-4\pi\chi$ with Meissner fractions corresponding to $\sim 40\%$. Figure 9 demonstrates for the first time that charge-stripe order exists throughout the entire superconducting region of $La_{1.6-x}Nd_{0.4}Sr_xCuO_4$. Furthermore, the 100% wipeout indicates that the charge-stripe transition involves the *entire* CuO_2 plane.

Figure 9 clearly indicates that T_{charge} for $La_{1.6-x}Nd_{0.4}Sr_xCuO_4$ does not strictly coincide with $T_{LTT}\sim 60$ K except at $x=0.12$, suggesting that the LTO-LTT structural transition is not the primary cause of the charge anomaly at T_{charge}. Further support of this statement comes from NQR wipeout measurements we made on $La_{1.8-x}Eu_{0.2}Sr_xCuO_4$ with $x=0.07$, 0.12, 0.16, and 0.20 all with LTO-LTT structural transition temperature $T_{LTT}\sim 130$ K (Ref. 34) that are higher than for $La_{1.6-x}Nd_{0.4}Sr_xCuO_4$ where $T_{LTT}\sim 60$ K. We used exactly the same techniques to measure $F(T)$ and T_{charge} for $La_{1.8-x}Eu_{0.2}Sr_xCuO_4$ as described earlier for $La_{1.6-x}Nd_{0.4}Sr_xCuO_4$, and the results shown in Fig. 9 indicate that $T_{charge}(x)$ for $La_{1.8-x}Eu_{0.2}Sr_xCuO_4$ and $La_{1.6-x}Nd_{0.4}Sr_xCuO_4$ is the same within the experimental error. This clearly shows that T_{charge} and T_{LTT} are not strictly correlated and that the LTT structural transition is not the primary origin of the charge anomaly. We also note that spin-stripe order has been observed in $La_{2-x}Sr_xCuO_4$ [$x=0.12$ (Refs. 2,3) and $x=0.05$ (Ref. 4)] and $La_2CuO_{4+\delta}$,[5] where neither material even has the LTO-LTT structural phase transition.

B. ^{63}Cu spin-lattice relaxation rate $^{63}1/T_1$

We now compare the temperature dependence of $^{63}1/T_1$ in $La_{1.48}Nd_{0.4}Sr_{0.12}CuO_4$, $La_{1.45}Nd_{0.4}Sr_{0.15}CuO_4$, $La_{1.68}Eu_{0.2}Sr_{0.12}CuO_4$, and $La_{1.885}Sr_{0.115}CuO_4$,[23] in light of previous $^{63}1/T_1$ measurements by Itoh *et al.*[35] on a variety of the rare earth (R) doped 1-2-3 materials $RBa_2Cu_3O_{7-y}$ [R = Y, Nd, Eu].

As discussed in Ref. 35, the $4f$ electron moments from the trivalent rare earth R^{3+} ions contribute to the $^{63}1/T_1$ primarily through a dipole interaction between the $4f$ moment and the Cu nuclear moment, giving the general form

$$^{63}1/T_1=(1/T_1)_{4f}+(1/T_1)_{Cu}. \quad (3)$$

We find that the $^{63}1/T_1$ data for $La_{1.885}Sr_{0.115}CuO_4$, $La_{1.6-x}Nd_{0.4}Sr_xCuO_4$, and $La_{1.68}Eu_{0.2}Sr_{0.12}CuO_4$ have the same systematic features as the equivalent $YBa_2Cu_3O_{7-y}$, $NdBa_2Cu_3O_{7-y}$, and $EuBa_2Cu_3O_{7-y}$ data.

(1) $La_{1.885}Sr_{0.115}CuO_4$ and $YBa_2Cu_3O_{7-y}$ have no $(1/T_1)_{4f}$ component, and $(1/T_1)_{Cu}$ for the observable segments of the NQR signal in $La_{1.885}Sr_{0.115}CuO_4$ decreases with decreasing temperature.[36]

(2) $La_{1.48}Nd_{0.4}Sr_{0.12}CuO_4$, $La_{1.45}Nd_{0.4}Sr_{0.15}CuO_4$, and $NdBa_2Cu_3O_{7-y}$ all have Nd^{3+} ions which have $J=9/2$ ground states, and a large $(1/T_1)_{4f}$ contribution is apparent with decreasing temperature in both cases. The temperature dependence of $(1/T_1)_{4f}$ depends on the details of the crystal field.[35] $(1/T_1)_{4f}$ for $NdBa_2Cu_3O_{7-y}$ is temperature independent down to at least 1 K, which is the expected behavior in the limit $T_N \ll T \ll \triangle_1$ where $T_N=0.52$ K is the ordering temperature and $\triangle_1=140$ K is the crystal field splitting between the ground state and the first excited state. The $La_{1.48}Nd_{0.4}Sr_{0.12}CuO_4$ and $La_{1.45}Nd_{0.4}Sr_{0.15}CuO_4$ data show that $(1/T_1)_{4f}$ increases with decreasing temperature, indicating that $\triangle_1 < 140$ K in these materials.

(3) $La_{1.68}Eu_{0.2}Sr_{0.12}CuO_4$ and $EuBa_2Cu_3O_{7-y}$ both have Eu^{3+} ions which have $J=0$ ground states and $J=1$ first excited states split by the spin-orbit constant λ. The $EuBa_2Cu_3O_{7-y}$ data show negligible $(1/T_1)_{4f}$ contribution at and below 50 K, consistent with the $\lambda=450$ K $\gg T$.[35] Since the first excited state is predominantely split by spin-orbit effects, one also expects negligible $(1/T_1)_{4f}$ contributions in $La_{1.68}Eu_{0.2}Sr_{0.12}CuO_4$ below 50 K. However, as the $La_{1.68}Eu_{0.2}Sr_{0.12}CuO_4$ data indicate, there is an increase in $^{63}1/T_1$ below 35(5) K, suggesting that the observable ^{63}Cu NQR signal senses diverging low frequency spin fluctuations due to critical slowing down of Cu moments toward $T_{spin}=25$–27 K as observed by μSR (Ref. 37) for $La_{1.68}Eu_{0.2}Sr_{0.12}CuO_4$. Both μSR and NQR have similar inherent probing frequencies of $\sim 10^7$ Hz; thus one expects T_{spin} even for a glassy transition to be comparable for both measurements, as is the case for $La_{2-x}Sr_xCuO_4$ according to μSR (Refs. 38, 39) and ^{139}La NQR.[40,2,23] We also find that $^{63}1/T_1T$ in $La_{1.68}Eu_{0.2}Sr_{0.12}CuO_4$ decreases slightly below T_{charge} prior to the onset of critical divergence of $^{63}1/T_1T$ toward T_{spin}. Even though reduction of $^{63}1/T_1T$ is usually attributed to pseudogap in the spin excitation spectrum, it is not clear whether that is the case here. We emphasize that the reduction of $^{63}1/T_1T$ is found for the observable fraction of the CuO_2 planes, and that the unobservable fraction may have divergent $^{63}1/T_1$ at $T \lesssim T_{charge}$.

We would like to add that although in the case of $La_{1.6-x}Nd_{0.4}Sr_xCuO_4$ below $T=125$ K, $(1/T_1)_{4f}$ dominates over $(1/T_1)_{Cu}$ and no spin ordering can be inferred, μSR measurements report that there is spin-ordering at temperatures T_{spin} similar to $La_{1.8-x}Eu_{0.2}Sr_xCuO_4$. μSR measurements were obtained for $La_{1.48}Nd_{0.4}Sr_{0.12}CuO_4$,[15,41] where $T_{spin} \sim 30$ K, and a reduced value for $La_{1.45}Nd_{0.4}Sr_{0.15}CuO_4$ of $T_{spin} \sim 25$ K has also been reported.[15,42] It was also shown by μSR (Ref. 42) that $T_{spin} \sim 25$ K for $La_{1.85-y}Nd_ySr_{0.15}CuO_4$ is independent of the Nd concentration y for $0.3 \leqslant y \leqslant 0.6$.

Figure 9 includes the values of T_{spin} for $La_{1.6-x}Nd_{0.4}Sr_xCuO_4$ according to neutron scattering[13] and μSR.[15] No spontaneous magnetization is detected for $x=0.20$ by μSR down to 4 K in contrast to the static spin-stripe observations by neutron scattering,[13,12] where $T_{spin} \sim 20$ K for $x=0.20$. Indeed, for $x=0.10$, 0.12, 0.15, and 0.20, T_{spin} is consistently ~ 20 K higher for neutron scattering[13,12] than for μSR measurements.[15] Further evidence of the glassy nature of the spin-ordering comes from electron spin resonance studies by Kataev *et al.*[34] for $La_{1.8-x}Eu_{0.2}Sr_xCuO_4$ at $x \sim 1/8$, where they clearly observe that the Cu spin fluctuation frequency ω_{sf} shows a strong temperature dependence below T_{charge}.

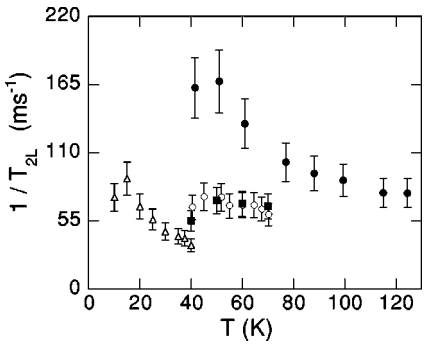

FIG. 10. Temperature dependence of $^{63}1/T_2$ in ms^{-1} for $La_{1.6-x}Nd_{0.4}Sr_xCuO_4$ with $x=0.07$ (●), $x=0.12$ (○), $x=0.25$ (△), and also for $La_{1.68}Eu_{0.2}Sr_{0.12}CuO_4$ (■).

C. ^{63}Cu spin-echo decay $^{63}1/T_2$

We now discuss the temperature dependence of the spin echo decay both above and below T_{charge}. Above T_{charge}, the spin-echo decay from all the samples were fit using the two free parameters T_{2G} and T_{2L} in Eq. (1). We found that greatly reducing the excitation range from ~ 200 kHz to ~ 50 kHz caused a significant reduction of the Gaussian component. This can be understood[25] in the context of inhomogeneous broadening, where reducing the frequency range has the effect of reducing the number of like spins responsible for the indirect spin-spin (Gaussian) decay. The reverse situation where the frequency range is kept fixed but the inhomogeneous line is broadened will also reduce the number of like spins. Either way, detuning the spin-spin mechanism[25] results in an apparent reduction of the Gaussian curvature in the spin-echo envelope and results in the Gaussian contribution to the second moment appearing more Lorentzian in character. However, even if we used weak rf pulses and thereby eliminate the Gaussian curvature in the spin-echo decay, we found that the extrapolated value $S(0)$ does *not* change.

Even though the NQR HWHM does not increase significantly around T_{charge} [Fig. 2(a)] and we maintain the same strength of rf pulses, we still observed a dramatic reduction of the Gaussian component at and below T_{charge}, indicating that there *is* a mechanism below T_{charge} that inherently eliminates the Gaussian process. The same mechanism that causes the wipeout can also be used to explain the crossover, namely, that the spatial charge modulations below T_{charge} detune the indirect interaction by creating site to site $^{63}\nu_Q$ variations, thereby reducing the number of like spins and thus eliminating the Gaussian decay. Below T_{charge}, the

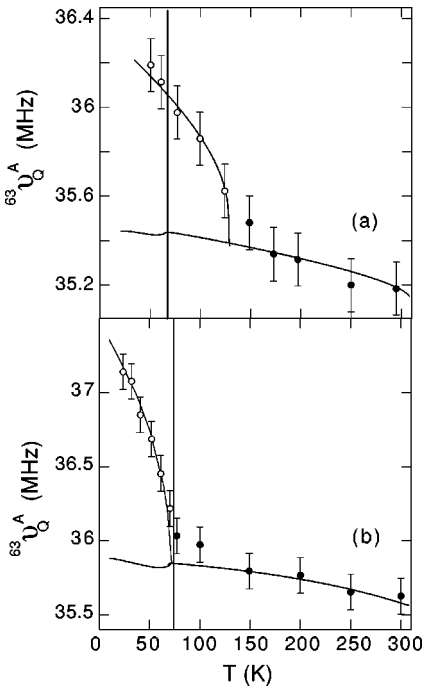

FIG. 11. Temperature dependence of $^{63}\nu_Q$ A line for (a) $x=0.07$ and (b) $x=0.12$. (●) corresponds to data for $T>T_{charge}$ and (○) to $T<T_{charge}$. The vertical line indicates the LTO-LTT transition temperature. The upper curve of the fit corresponds to finite $\Phi_t(x)$, and the lower curve to $\Phi_t(x)=0$.

spin-echo decay was always Lorentzian with $T_{2L} \ll T_1$. We observed that reducing the spectral excitation range in this case did *not* change T_{2L}. Figure 10 shows the temperature dependence of $^{63}1/T_{2L}$ for a selection of the $La_{1.6-x}Nd_{0.4}Sr_xCuO_4$ samples and $La_{1.68}Eu_{0.2}Sr_{0.12}CuO_4$.[1] The data at each doping start at T_{charge} and finish when the wipeout is nearly complete. The doping dependence of $^{63}1/T_{2L}$ shows a systematic decease with increased hole doping x. If $^{63}1/T_{2L}$ was entirely dominated by $4f$ moment fluctuations from the Nd^{3+} ion, $^{63}1/T_{2L}$ would not show this doping dependence. Moreover, as argued for the $^{63}1/T_1$ data, $La_{1.68}Eu_{0.2}Sr_{0.12}CuO_4$ has a negligible $4f$ moment at 50 K, yet within scattering, $^{63}1/T_{2L}$ at 50 K is the same as for $La_{1.48}Nd_{0.4}Sr_{0.12}CuO_4$.

The fact that $T_{2L} \ll T_1$, coupled with the fact that the Nd^{3+} ion is not the primary source of relaxation, leads us to believe that within the observable domains there exist certain magnetic hyperfine fields H_{hf} at the Cu site that fluctuate with a correlation time τ_c satisfying the motional narrowing limit $\gamma_n H_{hf} \tau_c \ll 1$ (Ref. 17) (where γ_n is the Cu gyromagnetic ratio). We infer that these fluctuations are primarily magnetic rather than quadrupolar by verifying that

$$\frac{^{65}1/T_{2L}}{^{63}1/T_{2L}} \sim \frac{^{65}\gamma_n^2}{^{63}\gamma_n^2} = 1.15. \tag{4}$$

The frequency dependence of $1/T_{2L}$ for the $x=0.20$ sample was shown in Fig. 4(a) at $T=30$ K$\ll T_{charge}$, and indeed, the 15% rise at lower frequency is consistent with primarily magnetic relaxation. It is also known that in the motional narrowing limit[17]

TABLE I. Experimentally determined values of $\Phi_0(x)$ in degrees,[47] and theoretically determined values of $\Phi_t(x)$ in degrees (see text) for $x=0.07$ and $x=0.12$.

x	$\Phi_0(x)$	$\Phi_t(x)$
0.07	5.5°	4.5°
0.12	4.8°	4.5°

$$1/T_{2L} \sim \gamma_n^2 H_{hf}^2 \tau_c, \tag{5}$$

but since $\gamma_n H_{hf}$ is not known, one cannot estimate τ_c. We note, however, that a sliding motion of CDW's in conventional CDW conductors causes motional narrowing.[18] Our present case is unconventional in the sense that we are observing the fraction of the material that has not yet ordered, and that charge order turns on slow spin dynamics.[27]

D. Temperature dependence of $^{63}\nu_Q$

Figure 11 shows the temperature dependence of A line $^{63}\nu_Q$ for $x=0.07$ and 0.12. The closed symbols indicate temperatures above T_{charge}, and open symbols below T_{charge}. Also shown is the vertical line marking the structural transition temperature T_{LTT} from the LTO to LTT (or LTLO). We define T_{ν_Q} as the temperature below which the rise in the A line $^{63}\nu_Q$ for the observable part of the signal starts to increase. $T_{\nu_Q}=70(7)$ K for $x=0.12$ and $T_{\nu_Q}\approx 130(13)$ K for $x=0.07$. T_{HTT} is also defined as the high-temperature tetragonal (HTT) to LTO transition temperature.[43]

The measurement of the temperature dependence for the A line $^{63}\nu_Q$ for $x>0.12$ has an added complexity to it. As shown in Fig. 1(a), the B line increases in amplitude with Sr doping, and unfortunately, the B line ^{65}Cu frequency coincides with the main A line ^{63}Cu. This is evident in Fig. 4(a) for $x=0.20$ where the shape of the main peak is largely due to the ^{65}Cu B line. Accurate determination of the A line $^{63}\nu_Q$ temperature dependence therefore implies taking very careful line shapes of a decreasing signal intensity below T_{charge}. We have however been able to determine that the A line $^{63}\nu_Q$ for all the samples increases with decreasing temperature down to ~ 10 K and that the rise below $T_{\nu_Q}=70(7)$ K is sharp for $x=0.12$. $x=0.09$ and 0.12 have qualitatively the same temperature dependence of the A line $^{63}\nu_Q$.

There are at least two possible explanations for the sharp rise in $^{63}\nu_Q$ below T_{ν_Q} for $x=0.12$. One is based on electronic effects. If we assume that T_{ν_Q} is in the vicinity of T_{charge}, which is certainly true for $x=0.12$, one can postulate that regions with lower hole concentrations wipe out at higher temperatures in such a way that $^{63}\nu_Q$ will appear to increase with decreasing temperature (recall that regions with higher hole concentrations have higher $^{63}\nu_Q$ values).

Another possible explanation for the large rise in $^{63}\nu_Q$ arises from structural distortion. In order to obtain a semiquantitative idea of how structural effects change $^{63}\nu_Q$, we calculate the electic field gradient at the Cu site by a point charge lattice summation method similar to that reported in Ref. 44. The two inputs necessary for the EFG calculation are the positions of the ions ($\mathbf{r}_i$) relative to the Cu nucleus

and the point charge of the ions (e_i). The lattice components of the EFG are calculated from summations such as

$$eq^{z}_{latt}=\sum_{\mathbf{i}} e_i \frac{(3z_i^2-r_i^2)}{r_i^5}, \tag{6}$$

where we included all the ions within a sphere of radius 100 Å from the origin. The ionic charges for the A line are assigned as follows:

$$\mathrm{La(Nd)}:+3, \quad \mathrm{O}_p:-\left(2-\frac{x}{2}\right), \quad \mathrm{O}_a:-2, \quad \mathrm{Cu}:+2, \tag{7}$$

where O_p is the planar oxygen and O_a the apical oxygen. The room temperature values of the lattice constants are taken from high resolution x-ray diffraction.[45] With decreasing temperature, the percentile change of the lattice constants are taken from Ref. 46, where the orthorhombic splitting is reported to go as

$$[b-a](x,T)\sim[b-a]_0(x)\times(1-T/T_{HTT})^{2\beta}, \tag{8}$$

where $\beta=1/3$. The oxygen octahedron tilting angle is taken to have the form[47]

$$\Phi(x,T)\sim\Phi_0(x)\times(1-T/T_{HTT})^{\beta}, \tag{9}$$

also with $\beta=1/3$. Below T_{LTT}, $[b-a]$ is set to zero, and Φ is kept at its maximum angle $\Phi_0(x)$, whose value is taken from Ref. 47.

For $^{63}\nu_Q$ in units of MHz and eq_{latt} in units of emu $\times 10^{14}$, $^{63}\nu_Q$ has the general empirical form[44]

$$^{63}\nu_Q=A(x)-B\times eq_{latt}(x,T), \tag{10}$$

where $A(x)$ ($\approx$70 MHz) is the contribution from the hole in the $3d_{x^2-y^2}$ orbital and its value was chosen to match the room temperature value of the A line $^{63}\nu_Q$. B is determined by antishielding effects[17] and the value is estimated to be 14.1 MHz from an empirical fit performed by Shimizu *et al.* on a large pool of data for different superconducting materials. Our calculations typically give $eq_{latt}\approx 2.7$, consistent with lattice EFG's for high-T_c cuprates.[44] We note that the only parameter we have adjusted to best fit the data is the constant $A(x)$. All the other parameters have been taken from other experimental sources.

We can check that the calculation is in semiquantitative agreement with the data by confirming the monotonic rise in $^{63}\nu_Q$ with deceasing temperature in the LTO phase (without tilting the octahedra, the calculation predicts that $^{63}\nu_Q$ *decreases* due to lattice shrinking). Indeed the calculation does show semiquantitative agreement with the data above T_{ν_Q}.

An important result from the calculation is that the change from LTO to LTT has little effect on $^{63}\nu_Q$, i.e., $^{63}\nu_Q$ is insensitive to azimuthal rotations of the octahedra about the c axis. This justifies the fact that we have neglected any intermediate LTLO phases.[33] However, $^{63}\nu_Q$ is sensitive to the angle that the octahedra are tilted from the c axis. Thus, in order to try to account for the dramatic increase of $^{63}\nu_Q$ below T_{ν_Q} for the observable NQR signal just from structural effects, we further tilted the octahedra from the c axis starting at T_{ν_Q} and we took the same temperature dependence of the angle in the LTO phase:

$$\Phi(x,T<T_{\nu_Q})\sim\Phi_0(x)+\Phi_t(x)\times(1-T/T_{\nu_Q})^{\beta}. \tag{11}$$

The only additional parameters now are the maximum tilt angle of the extra tilt called $\Phi_t(x)$, and T_{ν_Q}. It is clear for $x=0.12$ that $T_{\nu_Q}\sim T_{charge}=70(7)$ K, and for $x=0.07$ we have also used $T_{\nu_Q}\sim T_{charge}=130(13)$ K. The lower line in each plot is with $\Phi_t(x)=0$ and the upper line is for finite $\Phi_t(x)$. The rise in $^{63}\nu_Q$ can now be reproduced, and the angles used are shown in Table I.

We point out that the values of $\Phi_t(x)$ that best reproduce the data should only be taken as estimates. The calculation so far described is naturally very sensitive to the exact ion positions and to the constant B. For instance, using a larger B will make $^{63}\nu_Q$ more sensitive to changes in eq_{latt}, and one would then use lower values of $\Phi_t(x)$ to reproduce the data.

There is no conclusive evidence either way. We are reminded however that neither possibility has to involve all segments, just those that have not yet been wiped out. Even though there have been no reports from bulk scattering experiments[47,33] that there is further octahedron tilting at temperatures below T_{LTT}, bulk scattering experiments[47,33] measure the spatial average of the tilting angle while $^{63}\nu_Q$ is a local probe of the observable segments.

Using the same method as described above, we also calculated the effects charge-stripe formation alone would have on the EFG for $x=1/8$. First, we confirmed that adding 0.5 hole uniformly on the planar oxygens can account for the rise in the A line $^{63}\nu_Q$ of $\sim$8 MHz, in agreement with experimental observations in $La_{2-x}Sr_xCuO_4$.[22] Next, we took the conventional stripe picture[7] where the holes lie uniformly in the river of holes across one Cu chain separated by bare three leg ladders, and we predicted an NQR line splitting into the three peaks corresponding to the three distinct Cu sites (actually each peak was further split $\sim$300 kHz into two due to perpendicular stripes from neighboring planes). In the calculation, we interpreted one hole on a Cu site to mean one hole distributed evenly around its four surrounding planar oxygens. The highest frequency peak corresponding to the Cu site on the river shifted $\sim$6 MHz above the uniformly doped case, while the lowest peak corresponding to the Cu at the center of the three-leg ladder shifted $\sim$3 MHz below the uniform case. We also tried various charge-stripe configurations,[48] and we found that any smoothing of the charge distribution reduced the peak splitting.

Contrary to these calculated results of $^{63}\nu_Q$ in stripes, no NQR line splitting for the observable part of the signal was observed experimentally at or below T_{charge}. This implies that there is no static stripe order in the observable part of the CuO_2 plane. The signal we can observe below T_{charge} is either from islands that have not yet ordered, or from islands with quasistatic order but with NQR lines that are motionally narrowed.

IV. CONCLUSIONS

In this paper, we have reported a systematic study of the temperature and doping dependence of stripe instabilities in

$La_{1.6-x}Nd_{0.4}Sr_xCuO_4$ throughout the superconducting regime based on ^{63}Cu NQR. Our approach takes advantage of the extreme sensitivity of ^{63}Cu NQR to charge stripes. We have confirmed that the NQR wipeout fraction $F(T)$ is a good measure of the charge-stripe order parameter,[8–10] and we have extended earlier measurements of the charge-stripe order parameter based on diffraction techniques beyond $x=0.12,0.15$ to $0.07 \leqslant x \leqslant 0.25$, and, in doing so, obtain an extended phase diagram of the $La_{1.6-x}Nd_{0.4}Sr_xCuO_4$ system. We have also presented and discussed the temperature and doping dependence of the NQR parameters $^{63}\nu_Q$, $^{63}1/T_1$, and $^{63}1/T_2$.

We have shown that robust charge-stripe order continues to hold up to $x=0.25$, where no static hyperfine fields have been reported by μSR. This implies that completely static spin ordering is *not* a necessity for charge ordering. On the other hand, the Lorentzian spin-spin relaxation rate $^{63}1/T_{2L}$ observed below T_{charge} suggests that charge stripes continue to fluctuate slowly even below T_{charge}.

Our observation that T_{charge} is higher for lower doping x is counterintuitive, given that the charge-stripe transition is sharpest for $x=1/8$. On the other hand, the lower the hole concentration x, the stronger the tendency towards charge localization. This might explain why the onset of charge order is as much as a factor of 2 higher in temperature for $x=0.07$ than for $x=0.12$. We should also recall that NQR is a local probe sensitive to stripes no matter how they are disordered.

Comparison of the stripe-superconductivity phase diagram of $La_{1.6-x}Nd_{0.4}Sr_xCuO_4$ with our results obtained for $La_{2-x}Sr_xCuO_4$ (Ref. 1) reveals a possibly striking feature: it would appear that charge-stripe order stops when T_{charge} becomes lower than T_c, which for $La_{2-x}Sr_xCuO_4$ happens to occur at $x \sim 1/8$, but for $La_{1.6-x}Nd_{0.4}Sr_xCuO_4$ does not happen due to the highly suppressed T_c and the larger T_{charge}. A natural question to ask is whether the stripe instabilities and superconductivity compete. If one looks at the $La_{2-x}Sr_xCuO_4$ with $x>1/8$, where static-stripe ordering is suppressed and superconductivity is robust, one may conclude they compete with each other. However, inelastic neutron scattering measurements[27] indicate that low energy ($\gtrsim 2$ meV) dynamic stripe fluctuations extend beyond $x=1/8$, and perhaps they coexist even in $YBa_2Cu_3O_{6.6}$.[49] Furthermore, neutron scattering on $La_2CuO_{4+\delta}$ by Lee *et al.*[5] report that the elastic spin-order intensity appears at the same temperature as the superconductivity, suggesting that the two phenomena are strongly correlated. Our new stripe-superconductivity phase diagram for $La_{1.6-x}Nd_{0.4}Sr_xCuO_4$ in Fig. 9 also clearly indicates that the superconductivity phase boundary exists within the charge-stripe phase boundary.

ACKNOWLEDGMENTS

We thank K. R. Thurber, Y. S. Lee, R. J. Birgeneau, M. A. Kastner, J. M. Tranquada, and V. J. Emery for valuable discussions. This work was supported by NSF Grant No. DMR 99-71266, NSF Grant No. DMR 98-08941, and in part by the A.P. Sloan Foundation and the Mitsui Foundation. One of us (P.M.S.) has been supported by the Platzmann Fund during the course of this study.

[1] A.W. Hunt, P.M. Singer, K.R. Thurber, and T. Imai, Phys. Rev. Lett. **82**, 4300 (1999).

[2] T. Suzuki, T. Goto, K. Chiba, T. Shinoda, T. Fukase, H. Kimura, K. Yamada, M. Ohashi, and Y. Yamaguchi, Phys. Rev. B **57**, R3229 (1998).

[3] H. Kimura, K. Hirota, H. Matsushita, K. Yamada, Y. Endoh, S.-H. Lee, C. F. Majkrzak, R. Erwin, G. Shirane, M. Greven, Y.S. Lee, M.A. Kastner, and R. J. Birgeneau, Phys. Rev. B **59**, 6517 (1999).

[4] S. Wakimoto, G. Shirane, Y. Endoh, K. Hirota, S. Ueka, K. Yamada, R.J. Birgeneau, M.A. Kastner, Y.S. Lee, P.M. Gehring, and S.H. Lee, Phys. Rev. B **60**, R769 (1999).

[5] Y.S. Lee, R.J. Birgeneau, M.A. Kastner, Y. Endoh, S. Wakimoto, K. Yamada, R.W. Erwin, S.-H. Lee, and G. Shirane, Phys. Rev. B **60**, 3643 (1999).

[6] X.J. Zhou, P. Bogdanov, S. A. Kellar, T. Noda, H. Eisaki, S. Uchida, Z. Hussain, and Z.-X. Shen, Science **286**, 268 (1999).

[7] J.M. Tranquada, B.J. Sternlieb, J.D. Axe, Y. Nakamura, and S. Uchida, Nature (London) **375**, 561 (1995).

[8] J.M. Tranquada, J.D. Axe, N. Ichikawa, Y. Nakamura, S. Uchida, and B. Nachumi, Phys. Rev. B **54**, 7489 (1996).

[9] M.v. Zimmermann, A. Vigliante, T. Niemöller, N. Ichikawa, T. Frello, J. Madsen, P. Wochner, S. Uchida, N.H. Andersen, J.M. Tranquada, D. Gibbs, and J.R. Schneider, Europhys. Lett. **41**, 629 (1998).

[10] T. Niemöller, H. Hünnefeld, J.R. Schneider, N. Ichikawa, S. Uchida, T. Frello, N.H. Andersen, and J.M. Tranquada, cond-mat/9904383 (unpublished).

[11] T. Noda, H. Eisaki, and S. Uchida, Science **286**, 265 (1999).

[12] J.M. Tranquada, J.D. Axe, N. Ichikawa, A.R. Moodenbaugh, Y. Nakamura, and S. Uchida, Phys. Rev. Lett. **78**, 338 (1997).

[13] N. Ichikawa *et al.* (unpublished); N. Ichikawa, Ph.D. thesis, University of Tokyo, 1999.

[14] K. Yamada, C.H. Lee, K. Kurahashi, J. Wada, S. Wakimoto, S. Ueki, H. Kimura, Y. Endoh, S. Hosoya, G. Shirane, R.J. Birgeneau, M. Greven, M.A. Kastner, and Y.J. Kim, Phys. Rev. B **57**, 6165 (1998).

[15] B. Nachumi, Y. Fudamoto, A. Keren, K.M. Kojima, M. Larkin, G.M. Luke, J. Merrin, O. Tchernyshyov, Y.J. Uemura, N. Ichikawa, M. Goto, H. Takagi, S. Uchida, M.K. Crawford, E.M. McCarron, D.E. MacLaughlin, and R.H. Heffner, Phys. Rev. B **58**, 8760 (1998).

[16] A. Abragam, *Principles of Nuclear Magnetism* (Oxford University Press, Oxford, 1978).

[17] C.P. Slichter, *Principles of Magnetic Resonance*, 3rd ed. (Springer-Verlag, New York, 1989).

[18] J.H. Ross, Jr., Z. Wang, and C.P. Slichter, Phys. Rev. Lett. **56**, 663 (1986).

[19] K. Nomura, T. Sambongi, K. Kume, and M. Sato, Physica B & C **143**, 117 (1986).

[20] J. Winter, *Magnetic Resonance in Metals* (Oxford University Press, Oxford, 1971).

[21] M. Breuer, B. Büchner, R. Müller, M. Cramm, O. Maldonado, A. Freimuth, B. Roden, R. Borowski, B. Heymer, and D. Wohlleben, Physica C **208**, 217 (1993).
[22] K. Yoshimura, T. Uemura, M. Kato, K. Kosuge, T. Imai, and H. Yasuoka, Hyperfine Interact. **79**, 876 (1993).
[23] A.W. Hunt *et al.* (unpublished).
[24] C.H. Pennington, D.J. Durand, C.P. Slichter, J.P. Rice, E.D. Bukowski, and D.M. Ginsberg, Phys. Rev. B **39**, 274 (1989).
[25] D. Hone, V. Jaccarino, T. Ngwe, and P. Pincus, Phys. Rev. **186**, 291 (1969).
[26] S.W. Lovesey, *Theory of Neutron Scattering from Condensed Matter* (Oxford University Press, Oxford, 1984).
[27] J.M. Tranquada, N. Ichikawa, and S. Uchida, Phys. Rev. B **59**, 14 712 (1999).
[28] K.R. Thurber, T. Imai, T. Saitoh, M. Azuma, M. Takano, and F.C. Chou, cond-mat/9906141 (unpublished).
[29] H. Tou, M. Matsumura, and H. Yamagata, J. Phys. Soc. Jpn. **61**, 1477 (1992).
[30] G. Grüner, Rev. Mod. Phys. **60**, 1129 (1988).
[31] G. Grüner, *Density Waves in Solids* (Addison-Wesley, New York, 1994).
[32] We note that in the BCS dynamic limit, the temperature dependence of $f_d(T)$ is almost identical to that of the order parameter itself (Ref. 31), but it would be physically more accurate to associate $F(T)$ with $f_d(T)$.
[33] M.K. Crawford, R.L. Harlow, E.M. McCarron, W.E. Farneth, J.D. Axe, H. Chou, and Q. Huang, Phys. Rev. B **44**, 7749 (1991).
[34] V. Kataev, B. Rameev, A. Validov, B. Büchner, M. Hücher, and R. Borowski, Phys. Rev. B **58**, R11 876 (1998).
[35] M. Itoh, K. Karashima, M. Kyogoku, and I. Aoki, Physica C **160**, 177 (1989).
[36] T. Imai, C.P. Slichter, K. Yoshimura, and K. Kosuge, Phys. Rev. Lett. **70**, 1002 (1993).
[37] W. Wagener, H.-H. Klauss, M. Hillberg, M.A.C. de Melo, W. Kopmann, M. Birke, F.J. Litterst, B. Büchner, and H. Micklitz, J. Magn. Magn. Mater. **177**, 545 (1998).
[38] K.-I. Kumagi, K. Kawano, I. Watanabe, K. Nishiyama, and K. Nagamine, Hyperfine Interact. **86**, 473 (1994).
[39] Ch. Niedermayer, C. Bernhard, T. Blasius, A. Golnik, A. Moodenbaugh, and J.I. Budnick, Phys. Rev. Lett. **80**, 3843 (1998).
[40] F.C. Chou, F. Borsa, J.H. Cho, D.C. Johnston, A. Lascialfari, D.R. Torgeson, and J. Ziolo, Phys. Rev. Lett. **71**, 2323 (1993).
[41] G.M. Luke, K. Kojima, M. Larkin, J. Merrin, B. Nachumi, Y.J. Uemura, Y. Nakamura, S. Uchida, and M. Crawford, Hyperfine Interact. **105**, 113 (1997).
[42] W. Wagener, H.-H. Klauss, M. Hillberg, M.A.C. de Melo, M. Birke, F.J. Litterst, B. Büchner, and H. Micklitz, Phys. Rev. B **55**, R14 761 (1997).
[43] For details of the crystal structure, see D.M. Ginsberg, *Physical Properties of High Temperature Superconductors I* (World Scientific, Singapore, 1992).
[44] T. Shimizu, J. Phys. Soc. Jpn. **62**, 772 (1993).
[45] A.R. Moodenbaugh, L.H. Lewis, and S. Soman, Physica C **290**, 98 (1997).
[46] T. Suzuki and T. Fujita, J. Phys. Soc. Jpn. **6**, 1883 (1989).
[47] B. Buchner, M. Breuer, A. Freimuth, and A.P. Kampf, Phys. Rev. Lett. **73**, 1841 (1994).
[48] S.R. White and D.J. Scalapino, Phys. Rev. Lett. **80**, 1272 (1998).
[49] P. Dai, H.A. Mook, and F. Dogan, Phys. Rev. Lett. **80**, 1738 (1998).